IEEE Access
Multidisciplinary | Rapid Review | Open Access Journal

Received September 12, 2017, accepted October 13, 2017, date of publication November 2, 2017,
date of current version December 22, 2017.

Digital Object Identifier 10.1109/ACCESS.2017.2767638

Combined Constellation Rotation With Weighted FRFT for Secure Transmission in Polarization Modulation Based Dual-Polarized Satellite Communications

ZHANGKAI LUO[1], HUALI WANG[1], (Member, IEEE), KAIJIE ZHOU[1], AND WANGHAN LV[2]
[1]College of Communications Engineering, PLA Army Engineering University, Nanjing 210007, China
[2]School of Electronic and Optical Engineering, Nanjing University of Science and Technology, Nanjing 210094, China

Corresponding author: Zhangkai Luo (luo_zhangkai@126.com)

ABSTRACT In this paper, a novel transmission scheme based on constellation rotation and weighted fractional Fourier transform (WFRFT) is proposed to enhance the physical-layer security in polarization modulation (PM)-based dual-polarized satellite communications. Typically, by appropriately selecting the WFRFT order, the distribution of the signals processed by WFRFT can be close to Gaussian, which makes them difficult to be detected by eavesdroppers. However, once the signals are captured, it is possible for eavesdroppers to recover the information through the WFRFT order scanning method. To overcome this problem, in the proposed scheme, the constellation points are randomly rotated before the WFRFT operation, making it almost impossible to crack the WFRFT order. In this manner, the constellations are distorted, which is difficult for the eavesdropper to demodulate the signals accurately. Furthermore, a robust nonzero secrecy capacity is guaranteed. In addition, the impairment to the PM from the polarization-dependent loss effect is discussed, and a zero-forcing prefilter is applied at the receiver side to mitigate this adverse effect. Finally, the security performance of the proposed scheme is evaluated in terms of the average secrecy capacity and symbol error rate by numerical simulations in dual-polarized satellite communications.

INDEX TERMS Physical-layer secure transmission, weighted fractional Fourier transform, polarization state modulation, dual-polarized satellite communication.

I. INTRODUCTION

Satellite communication plays an important role in global communication networks and the transmission efficiency needs to increase to meet the ever-increasing data demand. In recent years, the application of multi-input multi-output (MIMO) techniques to satellite systems has received increasing attention [1]. However, MIMO techniques applied in satellite systems are different from terrestrial versions as the satellite channels comprise a line-of-sight (LOS) component, which will lead to correlation of the spatial components at the receiver side, even if the transmitting antennas are separated at half wavelength. Furthermore, without sufficient scatterings, the receiver can only discover a single transmission path, as its sensitivity is not sufficient to distinguish the different spatial signatures. Hence, such MIMO gains are hardly available as these gains depend on the decorrelation between channels [2].

Fortunately, orthogonal polarized channels provide more diversity and can be applied in satellite scenarios [3]. As an advanced technique, dual-polarized MIMO has been widely applied in most satellite communication systems. For instance, reference [4] demonstrated the dual-polarized MIMO channel was richer in terms of diversity. In [2] and [5], orthogonal polarization multiplexing (OPM) had been used to enhance the spectrum efficiency. In [6], dual-polarized antennas were used to carry information and achieved an improvement in throughput of up to 100% with respect to existing deployments. In addition, the amplitude ratio and phase difference between two orthogonally polarized branch signals can be used to carry polarization domain information. Thus, the polarization modulation (PM) has been studied and implemented over satellites [7]–[9], which has brought the following advantages:

- PM was a kind of three-dimensional modulation technique that utilized the polarization state (PS) as the information bearing parameter [10], which can be combined with multiple phase shift keying (MPSK)/ multiple quadrature amplitude modulation (MQAM) techniques and, thus improved the transmission efficiency.
- Arbitrary polarization states can be generated after the power amplifier by Power Division Unit and Phase Shifting Unit. In this way, the power amplifier can operate in the linear region without suffering distortion, thus improved the energy efficiency [11], [12].

On the other hand, security is a fundamental problem in dual-polarized satellite communications because of its broadcasting nature and wide beam coverage, which make it difficult to shield transmitted signals from eavesdroppers [13]. Transmission security is traditionally enhanced by cryptographic techniques in the link and network layers [14], which rely on computationally unbreakable mathematical manipulations. However, the high performance of CUP makes cryptography a less than ideal solution. In recent years, exploiting physical-layer characteristics for secure transmissions has become an emerging hot topic in wireless communications. New research has pointed out that a positive secrecy rate can guarantee ''perfect security'' even if the eavesdropper has unlimited computational capabilities [15]. Based on information theory, a positive secrecy rate can be achieved when authorized users obtain a higher signal-to-noise ratio (SNR) than the eavesdroppers [16]. However, it is not always the case in dual-polarized satellite communications, as two components of the polarized signal are transmitted by both two polarized channels and there is no extra degree of freedom to realize beamforming or insert artificial noise to worsen the eavesdropper's channel. Instead of relying on the uncontrollable channel features, the weighted fractional Fourier transform (WFRFT) was performed in [17] and [18] to safeguard the physical-layer security. As introduced in [19], WFRFT is a hybrid scheme of weighted single-carrier and multi-carrier modulation, which can adjust the distribution of the signals on demand. If the distribution was close to Gaussian, the signals were difficult to be detected. In [20], the traditional modulation signals were used to carry the normal information and the confidential messages were concealed in the polarization state (PS) of the signals. By appropriately designing the polarization modulation constellation and selecting the WFRFT order, the low detection probability performance can be improved. Then, through randomly changing the WFRFT order, the low probability of intercepted performance can be enhanced. However, once the WFRFT signals are captured by the eavesdropper, it is possible to demodulate the signals through scanning the WFRFT order.

In this paper, a more practical condition is assumed in which the confidential message is carried by both the traditional modulation and polarization modulation signals. Moreover, we assume the eavesdropper can capture the transmitted signals and has the information about the modulation techniques, so that it is possible for the eavesdropper to demodulate the signals accurately through scanning the WFRFT orders. To overcome this problem, the transmission security under these conditions is enhanced by the proposed transmission scheme, which is based on constellation rotation and weighted fractional Fourier transform (CR-WFRFT). At first, a constellation rotation method is designed to rotate the constellation points, such that the constellation points vary randomly. Then, after processing by WFRFT, the signals are transformed into quasi-Gaussian signals, which are difficult to be detected. For the eavesdropper, even if the signals are captured, it is almost impossible to demodulate the signals through scanning the WFRFT orders. This is because the signals after performing the inverse WFRFT operation are randomly distributed. Therefore, it is difficult to crack the WFRFT orders. Furthermore, the scanning errors of the WFRFT order will cause self-interferences at the eavesdropper side, which lead to the SNR degradation. In this way, a positive average secrecy capacity can be achieved and chosen for further enhancing the transmission security. In addition, the performance of PM will degrade due to the polarization dependent loss effect (PDL) from the dual-polarized satellite channel. To solve this problem, a zero-forcing prefilter is utilized to process the received signals at the receiver side. Finally, the security performance of the proposed scheme is evaluated in terms of both average secrecy capacity and symbol error rate (SER) by numerical simulations.

The rest of this paper is organized as follows: in Section II, the definition and properties of WFRFT is introduced. In Section III, the system model is introduced, then the characteristics of satellite depolarization channel model and the signal demodulation method are described. After that the transmission security benefits from WFRFT and its disadvantages are discussed. In Section IV, the principle of the CR-WFRFT scheme is described in detail. Simulation results are presented in Section V. Finally, Section VI concludes this paper.

Notations: The superscript T and H are used to denote the transpose and the Hermitian transpose of a vector or matrix. Vectors and matrices are represented by bold lowercase or uppercase. E [•] denotes the expectation operation and |•| the modulus value.

II. WEIGHTED FRACTIONAL FOURIER TRANSFORMATION

In this section, the definition and properties of WFRFT are introduced [17], [21].

Definition 1: For an arbitrary complex signal vector $\mathbf{s} = [s_1, s_2, \cdots, s_K] \in \mathbb{C}^K$, the α-order WFRFT of $\mathbf{s}$ is defined as:

$$\mathcal{F}^a(\mathbf{s}) = \Psi_M^{\alpha}[\mathbf{s}] = \sum_{l=0}^{M-1} w_l(a)\, \mathbf{F}_K^{\frac{4l}{M}} \mathbf{s}, \tag{1}$$

where $M \geq 4$ denotes the number of the basic operators involved and $\mathbf{F}_K$ denotes the unitary Fourier matrix whose

elements satisfy

$$F_K(g_1, g_2) = \frac{1}{\sqrt{K}} e^{-\mathrm{j}2\pi g_1 g_2/K}, \quad g_1, g_2 \in (0, 1, \cdots, K-1). \tag{2}$$

Typically, $\mathbf{F}_K(g_1, g_2)$ indicates the specific element that is located at the g_1-th row and g_2-th column in the matrix. The weighting coefficients $\{w_l(\alpha)\}_{l=0}^{M-1}$ can be calculated by

$$w_l(\alpha) = \frac{1}{M} \frac{1 - \exp[-2\pi j(\alpha - l)]}{1 - \exp[-2\pi j(\alpha - l)/M]}, \tag{3}$$

Based on Eq. (1), we define $\mathbf{W}_M^\alpha = \sum_{l=0}^{M-1} w_l(\alpha) \mathbf{F}_K^{\frac{4l}{M}}$ as the α-order MWFRFT transformation matrix and the α-order MWFRFT signal is denoted by $\Psi_M^\alpha[\mathbf{s}]$. Then the following axioms can be gotten:

- Interchange axiom

$$\Psi_M^\alpha\left[\Psi_M^{-\alpha}[\mathbf{s}]\right] = \Psi_M^{-\alpha}\left[\Psi_M^\alpha[\mathbf{s}]\right] = \mathbf{s}. \tag{4}$$

- Boundary axiom

$$\Psi_M^0[\mathbf{s}] = \mathbf{s}, \quad \Psi_M^1[\mathbf{s}] = \mathrm{DFT}(\mathbf{s}). \tag{5}$$

- Additive axiom

$$\Psi_M^{\alpha+\beta}[\mathbf{s}] = \Psi_M^\alpha\left[\Psi_M^\beta[\mathbf{s}]\right] = \Psi_M^\beta\left[\Psi_M^\alpha[\mathbf{s}]\right]. \tag{6}$$

In particular, we just consider the condition that $M = 4$, since the analysis process is similar for M with other values. According to the properties of the Fourier matrix, $\mathbf{F}_K^{-1} = \mathbf{F}_K^H = \mathbf{P}_K\mathbf{F}_K$, the α-order 4WFRFT transformation matrix can be written as

$$\begin{aligned}\mathbf{W}_4^a &= w_0(a)\mathbf{I}_K + w_1(a)\mathbf{F}_K + w_2(a)\mathbf{P}_K + w_3(a)\mathbf{F}_K^{-1} \\ &= w_0(a)\mathbf{I}_K + w_1(a)\mathbf{F}_K + w_2(a)\mathbf{P}_K + w_3(a)\mathbf{P}\mathbf{F}_K,\end{aligned} \tag{7}$$

where $\mathbf{I}_K$ denote the $K \times K$ identity matrix and $\mathbf{P}_K$ denotes the shift matrix, which can be represented as:

$$\mathbf{P}_K = \begin{bmatrix} 1 & 0 & \cdots & 0 & 0 & 0 \\ 0 & 0 & \cdots & 0 & 0 & 1 \\ 0 & 0 & \cdots & 0 & 1 & 0 \\ \vdots & \vdots & 0 & \ddots & 0 & 0 \\ 0 & 0 & 1 & 0 & \cdots & 0 \\ 0 & 1 & 0 & 0 & \cdots & 0 \end{bmatrix}_{K\times K}. \tag{8}$$

As α is a real number and $w_l(\alpha) = w_l(\alpha + 4)$, thus, $\alpha \in [0, 4]$ or $\alpha \in [-2, 2]$.

III. SYSTEM MODEL

A satellite scenario with three participants is assumed, a transmitter Alice, a authorized receiver Bob and an eavesdropper Eve as shown in Fig. 1. In order to transmit or receive polarized signals, all of them are equipped with a dual-polarized antenna. As the signals are broadcast from Alice to both two receivers, the eavesdropper can recover the same information as Bob, thus the information is eavesdropped.

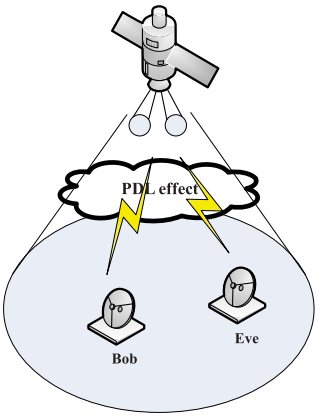

FIGURE 1. System model.

To prevent eavesdropping, the CR-WFRFT scheme is designed to enhance the transmission security. Particular descriptions are provided below.

A. SIGNAL MODEL AND CONSTELLATION STRUCTURE

The k-th transmit signal vector $\mathbf{x}_k$ can be written as [21]

$$\mathbf{x}_k = \begin{bmatrix} x_{\mathrm{H}k} \\ x_{\mathrm{V}k} \end{bmatrix} = \begin{bmatrix} \cos\gamma_k \\ \sin\gamma_k e^{j\eta_k} \end{bmatrix} A_k e^{j(w_c t + \varphi_k)}, \tag{9}$$

where $\gamma_k \in \left[0, \frac{\pi}{2}\right]$ is the amplitude relationship (or polarized angle) between the orthogonal dual-polarized components; $\eta_k \in [0, 2\pi]$ denotes the difference of them in phase; $A_k e^{j\varphi_k}$ denotes the M_q-th order amplitude-phase modulation signal (APM) and w_c is the carrier frequency. Hereafter, the signal in Eq. (9) is referred to as the PM-APM signal. $x_{\mathrm{H}k}$ and $x_{\mathrm{V}k}$ denote the horizontal component (H) and vertical component (V), respectively. The polarization state (PS) is defined as $\mathbf{P}_k = \begin{bmatrix} \cos\gamma_k \\ \sin\gamma_k e^{j\eta_k} \end{bmatrix}$.

The M_p-th order PM constellation structures used here are shown in Fig. 2: M_p equipower constellation points with the equal minimum constellation sphere distance d_{T} are placed symmetric to the g_1-axis of the unitary Poincare sphere and each constellation point denotes a unique PS.

B. POLARIZATION DEPENDENT LOSS EFFECT AND SIGNAL DEMODULATION

At the receiver side, the received signal can be represented as

$$\mathbf{y}_k = \begin{bmatrix} y_{\mathrm{H}k} \\ y_{\mathrm{V}k} \end{bmatrix} = \sqrt{P}\mathbf{H}\mathbf{x}_k + \mathbf{n}_k, \tag{10}$$

where $\mathbf{n}_k = \begin{bmatrix} n_{\mathrm{H}k} \\ n_{\mathrm{V}k} \end{bmatrix}$ is the noise vector with the probability density function (PDF) as $\mathcal{CN}\left(0, \sigma^2\mathbf{I}_{2\times 2}\right)$; P denotes the transmitting power; $\mathbf{H}$ denotes the satellite channel impulse response matrix, which can be further written as

$$\mathbf{H} = \begin{bmatrix} h_{11} & h_{12} \\ h_{21} & h_{22} \end{bmatrix} = \sqrt{\Upsilon}\mathbf{U}\Sigma\mathbf{V} = \sqrt{\Upsilon}\mathbf{U}\begin{bmatrix} \sqrt{\lambda_1} & 0 \\ 0 & \sqrt{\lambda_2} \end{bmatrix}\mathbf{V}, \tag{11}$$

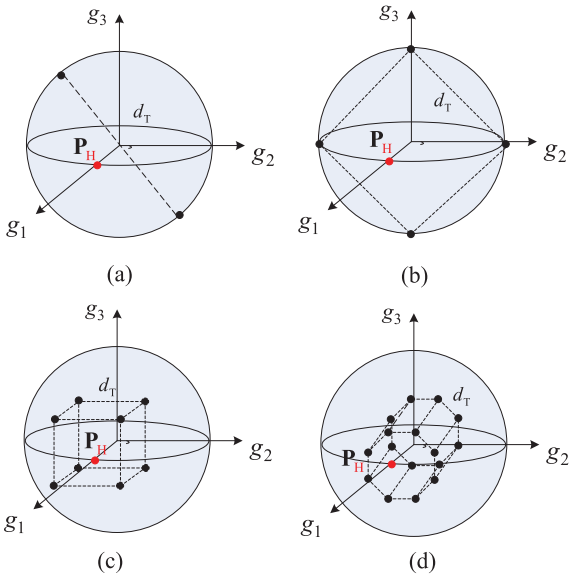

FIGURE 2. M_p-th order PM constellation structure. (a) 2PM. (b) 4PM. (c) 8PM. (d) 16PM.

where Υ is the power fading of the non-polarized channel and $\sqrt{\lambda_i}, i = 1, 2$ denote eigenvalues. $\mathbf{U}$ and $\mathbf{V}$ are unitary matrixes. Then, Eq. (10) can be further written as

$$\begin{aligned}\mathbf{Hx_k} &= \sqrt{\Upsilon}\mathbf{U}\begin{bmatrix}\sqrt{\lambda_1} & 0\\ 0 & \sqrt{\lambda_2}\end{bmatrix}\mathbf{V}\begin{bmatrix}\cos\gamma_k\\ \sin\gamma_k e^{j\eta_k}\end{bmatrix}A_k e^{j(w_c t+\varphi_k)}\\ &= \sqrt{\Upsilon}\mathbf{U}\begin{bmatrix}\sqrt{\lambda_1} & 0\\ 0 & \sqrt{\lambda_2}\end{bmatrix}\begin{bmatrix}\cos\gamma_k\\ \sin\gamma_k e^{j\tilde{\eta}_k}\end{bmatrix}A_k e^{j(w_c t+\varphi_k)}\\ &= \sqrt{\Upsilon}\mathbf{U}\begin{bmatrix}\sqrt{\lambda_1}\cos\gamma_k\\ \sqrt{\lambda_2}\sin\gamma_k e^{j\tilde{\eta}_k}\end{bmatrix}A_k e^{j(w_c t+\varphi_k)}\\ &= p_k\mathbf{U}\begin{bmatrix}\cos\tilde{\gamma}_k\\ \sin\tilde{\gamma}_k e^{j\tilde{\eta}_k}\end{bmatrix}A_k e^{j(w_c t+\varphi_k)}\\ &= p_k\begin{bmatrix}\cos\tilde{\gamma}_k\\ \sin\tilde{\gamma}_k e^{j\tilde{\eta}_k}\end{bmatrix}A_k e^{j(w_c t+\varphi_k)},\end{aligned} \tag{12}$$

where $\tilde{\gamma}_k = \arctan\left(\sqrt{\frac{\lambda_2}{\lambda_1}}\tan\gamma_k\right)$ and p_k is the normalization power factor as

$$p_k = \sqrt{P\Upsilon\left(\left(\sqrt{\lambda_1}\cos\gamma_k\right)^2 + \left(\sqrt{\lambda_2}\sin\gamma_k\right)^2\right)}. \tag{13}$$

From Eq. (12), we find that if $\lambda_1 \neq \lambda_2$, the PS of the polarized signal is changed and this is the PDL effect [12]. For a better understanding of the PDL effect, we utilize two constellation points ($\mathbf{P}_1, \mathbf{P}_2$) to illustrate the polarization transformation in Eq. (12). As shown in Fig. 3 on the Poincare ball [10], at first, affected by $\mathbf{V}$, $\mathbf{P}_1$ and $\mathbf{P}_2$ rotate as a rigid body, where the constellation distance is not changed and result in $\mathbf{P}_3$ and $\mathbf{P}_4$ without changing their power. This is because $\mathbf{U}$ is a unitary matrix, which creates a lossless polarization transfer. Then affected by Σ, they will move toward $\mathbf{P}_H$ as shown by $\mathbf{P}_5$ and $\mathbf{P}_6$ with their power changes into p_k. Finally, affected by $\mathbf{U}$, they will rotate as a rigid body and result in $\mathbf{P}_7$ and $\mathbf{P}_8$ without changing in their power. If $\mathbf{H}$ is an

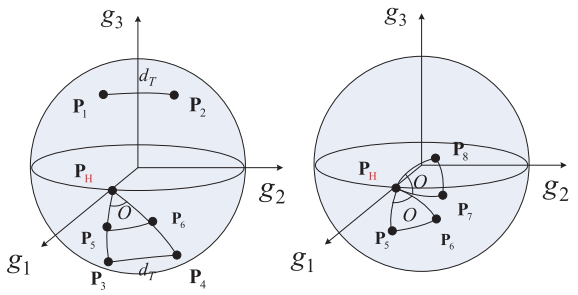

FIGURE 3. polarization transformation.

ideal channel with $\lambda_1 = \lambda_2 = 1$, then $\mathbf{P}_1 = \mathbf{P}_7$ and $\mathbf{P}_2 = \mathbf{P}_8$. The polarization parameters can be demodulated by

$$\begin{aligned}\gamma_{\mathrm{R}k} &= \arctan\left(\frac{\mathrm{abs}\,(y_{\mathrm{V}k})}{\mathrm{abs}\,(y_{\mathrm{H}k})}\right),\\ \eta_{\mathrm{R}k} &= \Xi\,(y_{\mathrm{V}k}) - \Xi\,(y_{\mathrm{H}k}).\end{aligned} \tag{14}$$

where Ξ is the phase acquisition function. Then the demodulated PS $\mathbf{P}_{\mathrm{D}k}$ can be obtained by

$$\mathbf{P}_{\mathrm{D}k} = \min_{1\le m\le M_p}\mathrm{dis}\,(\mathbf{P}_{\mathrm{R}k}, \mathbf{P}_{\mathrm{T}m}), \tag{15}$$

where $\mathbf{P}_{\mathrm{T}m}$ denotes the PS of the transmitted polarization constellation point; $\mathbf{P}_{\mathrm{R}k}$ denotes the PS of the k-th received signal; $\mathrm{dis}\,(\mathbf{P}_Z, \mathbf{P}_B)$ denotes the sphere distance between $\mathbf{P}_Z$ and $\mathbf{P}_B$, which can be calculated by

$$\mathrm{dis}\,(\mathbf{P}_Z,\mathbf{P}_B) = \arccos\begin{bmatrix}\cos(2\gamma_Z)\cos(2\gamma_B)\\ +\sin(2\gamma_Z)\sin(2\gamma_B)\sin(\eta_Z-\eta_B)\end{bmatrix}. \tag{16}$$

Then, the amplitude-phase modulation (APM) signal is obtained by performing the polarization match as

$$\begin{aligned}\mathbf{y}_k^{\mathrm{APM}} &= \begin{bmatrix}\cos\gamma_{\mathrm{R}k}\\ \sin\gamma_{\mathrm{R}k}e^{j\eta_{\mathrm{R}k}}\end{bmatrix}^{\mathrm{H}}\mathbf{y}_k\\ &= \left(\begin{array}{l}p_k\begin{bmatrix}\cos\gamma_{\mathrm{R}k}\\ \sin\gamma_{\mathrm{R}k}e^{j\eta_{\mathrm{R}k}}\end{bmatrix}^{\mathrm{H}}\begin{bmatrix}\cos\tilde{\gamma}_k\\ \sin\tilde{\gamma}_k e^{j\tilde{\eta}_k}\end{bmatrix}A_k e^{j(w_c t+\varphi_k)}\\ +\begin{bmatrix}\cos\gamma_{\mathrm{R}k}\\ \sin\gamma_{\mathrm{R}k}e^{j\eta_{\mathrm{R}k}}\end{bmatrix}^{\mathrm{H}}\mathbf{n}_k\end{array}\right).\end{aligned} \tag{17}$$

According to the ML demodulation rule, the APM signal can be demodulated. From Eq. (17), it is found that the demodulation of the APM signal is affected by the polarization match. If the noise effect is ignored, then $\cos\gamma_{\mathrm{R}k} = \cos\tilde{\gamma}_k$, $\eta_{\mathrm{R}k} = \tilde{\eta}_k$ and

$$\mathbf{y}_k^{\mathrm{APM}} = p_k A_k e^{j(w_c t+\varphi_k)}. \tag{18}$$

From Eq. (12) and Eq. (18), PM signal demodulation, under ideal channel conditions, is found to be only affected by the Gauss noise. However, if the channel condition is non-ideal, the demodulation performance of the PM signal will degrade due to the PDL effect, which further affect the APM signal demodulation performance. However, $\mathbf{H}$ is always non-ideal due to:

1. The cross-polarization discrimination (XPD) of the dual-polarized antenna at the receiver side is not large enough to ensure $h_{12} = h_{21} = 0$.

2. The complex electromagnetic environment, including the existing various clouds, rain, and ice crystals in the air, will cause signal refection, diffraction and diffuse scattering.

Consequently, the PSs of the received signal are always different from the transmit ones in most satellite scenarios, which limit the application of PM. Therefore, it is necessary to eliminate the PDL effect and the elimination method is described in section IV-B.

C. TRANSMISSION SECURITY BENEFITS FROM WFRFT AND DISADVANTAGES

In this section, to observe the security performance provided by WFRFT in dual-polarized satellite systems, an ideal channel condition is assumed. Moreover, the practical case is considered that the eavesdropper has the information regarding the modulation orders and constellation structures of both the PM and APM signals. If the signals are transmitted without any protection, they would be easily demodulated by the eavesdropper with the demodulation method described in the last section. Therefore, in this section, WFRFT is used to process the signals and then, we will analyze the security performance benefits from WFRFT and its disadvantages.

The transmit symbol matrix is denoted as

$$\mathbf{x} = [\mathbf{x}_1, \mathbf{x}_2, \cdots, \mathbf{x}_K] = \begin{bmatrix} \mathbf{x}_{\mathrm{H}} \\ \mathbf{x}_{\mathrm{V}} \end{bmatrix} = \begin{bmatrix} x_{\mathrm{H}1}, x_{\mathrm{H}2}, \cdots, x_{\mathrm{H}K} \\ x_{\mathrm{V}1}, x_{\mathrm{V}2}, \cdots, x_{\mathrm{V}K} \end{bmatrix}. \tag{19}$$

Then, the signal processed by α-order and β-order WFRFT are represented by $\Psi_4^{\alpha}(\mathbf{x}_{\mathrm{H}})$ and $\Psi_4^{\beta}(\mathbf{x}_{\mathrm{V}})$, respectively. As a promising signal processing technique, WFRFT can help to adjust the distribution of the transmitted signals on demand. By appropriately selecting α and β, the distribution of WFRFT signals could be close to Gaussian statistics, which yields the signals difficult to be detected, thus the transmission security is enhanced. The definition of Kurtosis is used here to measure the similarity between the WRFRT signals and the Gaussian signals [17].

Definition 2: For an arbitrary complex signal vector $\mathbf{x} = [x_1, x_2, \cdots, x_K] \in \mathbb{C}^K$, the Kurtosis of $\mathbf{x}$ is defined as:

$$J = \frac{E\left[\mathbf{x}^4\right]}{E\left[\mathbf{x}^2\right]^2} - 3. \tag{20}$$

If $J = 0$, the signals are Gaussian; if $J < 0$, the signals are sub-Gaussian; If $J > 0$, the signals are super-Gaussian.

The Kurtosis curves of both the real and imaginary parts of the WFRFT signals versus α are shown in Fig. 4. The V component of the PM-APM signal is taken as an example and the Kurtosis curves of different modulation order combinations are given in Fig. 4(a)- 4(d). It is found that for arbitrary modulation order combinations, we can always find the order α, which can transform the PM-APM signals into the quasi-Gaussian signals, which are difficult to detect even with a higher order statistics based classifier [18].

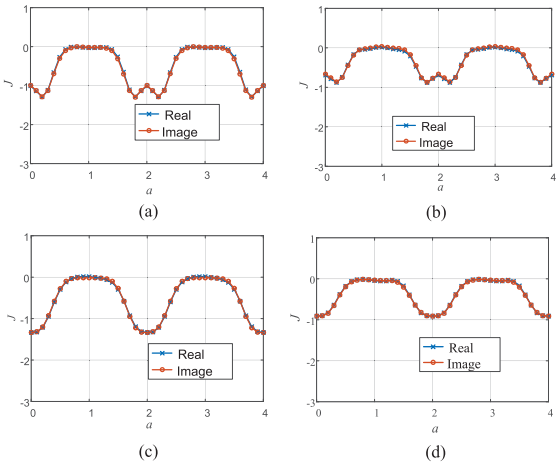

FIGURE 4. Kurtosis of WFRFT signals versus α. (a) QPSK with 4PM. (b) 16QAM with 4PM. (c) QPSK with 8PM. (d) 16QAM with 8PM.

However, once the signals are captured by the eavesdropper, it is possible for the eavesdropper to crack the WFRFT signals by scanning the WFRFT orders. Thus, the signals processed by inverse WFRFT are denoted as:

$$\begin{aligned} \mathbf{y}_{\mathrm{E}} &= \sqrt{P}\begin{bmatrix} \Psi_4^{\alpha_1}\left(\Psi_4^{\alpha}(\mathbf{x}_{\mathrm{H}})\right) \\ \Psi_4^{\beta_1}\left(\Psi_4^{\beta}(\mathbf{x}_{\mathrm{V}})\right) \end{bmatrix} + \begin{bmatrix} \Psi_4^{\alpha_1}(\mathbf{n}_{\mathrm{H}}) \\ \Psi_4^{\beta_1}(\mathbf{n}_{\mathrm{V}}) \end{bmatrix} \\ &= \sqrt{P}\begin{bmatrix} \Psi_4^{\Delta\alpha}(\mathbf{x}_{\mathrm{H}}) \\ \Psi_4^{\Delta\beta}(\mathbf{x}_{\mathrm{V}}) \end{bmatrix} + \begin{bmatrix} \hat{\mathbf{n}}_{\mathrm{H}} \\ \hat{\mathbf{n}}_{\mathrm{V}} \end{bmatrix}, \end{aligned} \tag{21}$$

where $\Delta\alpha = |\alpha - \alpha_1|$ and $\Delta\beta = |\beta - \beta_1|$ are scanning errors; $\hat{\mathbf{n}}_{\mathrm{H}}$ and $\hat{\mathbf{n}}_{\mathrm{V}}$ are noise vectors processed by WFRFT, whose PDFs are not changed as WFRFT is a kind of unitary transformation.

Fig. 5 shows the SER performance of both 4PM and QPSK signals versus scanning errors. In Fig. 5(a), the theoretical value is calculated by

$$SER_q = \begin{pmatrix} 2\left(1 - 1/\sqrt{M_q}\right)\mathrm{erfc}\left(\sqrt{\dfrac{3\xi\log_2\left(M_q\right)}{M_q - 1}}\right) \\ -\left(1 - 1/\sqrt{M_q}\right)^2\mathrm{erfc}^2\left(\sqrt{\dfrac{3\xi\log_2\left(M_q\right)}{M_q - 1}}\right) \end{pmatrix}, \tag{22}$$

where ξ denote the bit SNR. It is found that even with the inverse WFRFT orders $\alpha_1 = \beta_1 = -0.7$, the SER performance is still worse than the theoretical values. This is because the demodulation performance of the QPSK signals is affected by the polarization match. As shown by Eq. (17), if $\gamma_{\mathrm{R}k} \neq \tilde{\gamma}_k$, $\eta_{\mathrm{R}k} \neq \tilde{\eta}_k$, the amplitude and phase of the QPSK signals are changed, and thus the SER performance degrades. In Fig. 5(b), the calculation method of the theoretical values of the 4PM signals is provided in the Appendix.

From Fig. 5(a) and Fig. 5(b), it is found that the smaller the scanning errors, the better the SER performance and when $\Delta\alpha = \Delta\beta = 0.01$, the SER performance of the eavesdropper is almost the same as the authorized receiver. As $\alpha, \beta \in [0, 4]$, when the scan step is 0.01, it requires 1600 scans, the PM-APM signals are demodulated. To resist

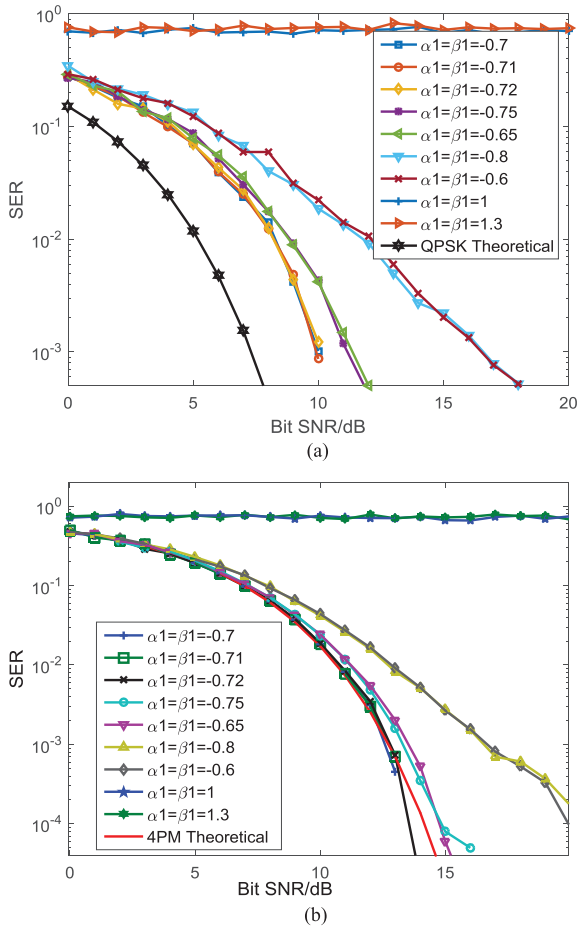

FIGURE 5. SER performance versus different scanning errors ($\alpha = \beta = 0.7$). (a) SER performance of the QPSK signal. (b) SER performance of the 4PM signal.

scanning decoding, an alterable-parameter 4WFRFT method has been proposed in [22], where the order α is divided into 8 groups and changed for every N symbol periods. Although this method makes the communication more reliable, it cannot totally prevent scanning decoding for the extremely high performance CPU nowadays. To solve the problem, the CR-WFRFT scheme is proposed, as described in the next section.

IV. PRINCIPLE OF THE CR-WFRFT SCHEME

As discussed in the last section, WFRFT signals can be eavesdropped through the WFRFT order scanning method, which is mainly due to the transmitted PM-APM signals being regularly distributed according to the constellation structures before performing WFRFT. Therefore, in this section, pseudo random symbol-specific rotation angles are suggested for different symbols, which are generated based on the pseudo sequence [23]. In this way, based on the assumption that the PN sequence is only shared between the transmitter Alice and the authorized receiver Bob, but could not be accessed by the eavesdropper, the eavesdropper can only obtain the randomly rotated signals by scanning the WFRFT orders. In this manner, the WFRFT orders are impossible to be cracked. The detailed analysis is described in this section.

A. PSEUDO RANDOM CONSTELLATION ROTATION

The pseudo random rotation angle assigned to the k-th symbol is $e^{j\theta_k}$, where θ_k is the symbol-specific rotation angle, which is generated by the pseudo random sequence generator. For the transmitted signal as shown by Eq. (9), two problems arise:

1. Which constellation is more suitable to be rotated, the APM constellation or the PM constellation ?

2. If the PM constellation is rotated, which polarized component is more appropriate to multiply with the rotation angle ?

To find out which strategy is the most effective, at first, the APM signal is multiplied with the rotation angle like the following:

$$\mathbf{x}_k^{\mathrm{r}} = \begin{bmatrix} x_{\mathrm{H}k}^{\mathrm{r}} \\ x_{\mathrm{V}k}^{\mathrm{r}} \end{bmatrix} = \begin{bmatrix} \cos\gamma_k \\ \sin\gamma_k e^{j\eta_k} \end{bmatrix} A_k e^{j(w_c t+\theta_k+\varphi_k)}. \tag{23}$$

Then, it is found that the phase of the APM signal varies randomly due to the random rotation angle θ_k, while the PS of the transmitted signal is not changed. Therefore, it is possible for the eavesdropper to get the information carried by the PS of the transmitted signal through the order scanning method.

Then, we consider the case that the PM constellation structure is rotated and the vertical component is multiply by the random rotation angle as:

$$\mathbf{x}_k^{\mathrm{r}} = \begin{bmatrix} x_{\mathrm{H}k}^{\mathrm{r}} \\ x_{\mathrm{V}k}^{\mathrm{r}} \end{bmatrix} = \begin{bmatrix} \cos\gamma_k \\ \sin\gamma_k e^{j(\eta_k+\theta_k)} \end{bmatrix} A_k e^{j(w_c t+\varphi_k)}. \tag{24}$$

It is found that the phase difference between the two components of the PM signal varies randomly, while the information carried by the APM signal may be eavesdropped. To simplified the analysis, the noise is ignored and an ideal channel condition is assumed, such that $\mathbf{y}_k = \mathbf{x}_k^{\mathrm{r}}$. Based on Eqs. (12) and (14), we obtain

$$\begin{aligned} \gamma_{\mathrm{R}k} &= \arctan\left(\frac{\mathrm{abs}\,(y_{\mathrm{V}k})}{\mathrm{abs}\,(y_{\mathrm{H}k})}\right) = \gamma_k, \\ \eta_{\mathrm{R}k} &= \Xi\,(y_{\mathrm{V}k}) - \Xi\,(y_{\mathrm{H}k}) = \eta_k + \theta_k. \end{aligned} \tag{25}$$

Then, based on Eq. (17), after performing the polarization match, the APM signal is directly demodulated as

$$\begin{aligned} \mathbf{y}_k^{\mathrm{APM}} &= \begin{bmatrix} \cos\gamma_{\mathrm{R}k} \\ \sin\gamma_{\mathrm{R}k} e^{j\eta_{\mathrm{R}k}} \end{bmatrix}^{\mathrm{H}} \mathbf{y}_k \\ &= \sqrt{P\Upsilon}\begin{bmatrix} \cos\gamma_{\mathrm{R}k} \\ \sin\gamma_{\mathrm{R}k} e^{j\eta_{\mathrm{R}k}} \end{bmatrix}^{\mathrm{H}} \begin{bmatrix} \cos\gamma_k \\ \sin\gamma_k e^{j(\eta_k+\theta_k)} \end{bmatrix} A_k e^{j(w_c t+\varphi_k)} \\ &= \sqrt{P\Upsilon} A_k e^{j(w_c t+\varphi_k)}. \end{aligned} \tag{26}$$

Thus, based on the order scanning method, it is possible for the eavesdropper to demodulate the APM signals.

Finally, the random rotation angle is multiply with the horizontal component as

$$\mathbf{x}_k^{\mathrm{r}} = \begin{bmatrix} x_{\mathrm{H}k}^{\mathrm{r}} \\ x_{\mathrm{V}k}^{\mathrm{r}} \end{bmatrix} = \begin{bmatrix} \cos\gamma_k e^{j\theta_k} \\ \sin\gamma_k e^{j\eta_k} \end{bmatrix} A_k e^{j(w_c t+\varphi_k)}. \tag{27}$$

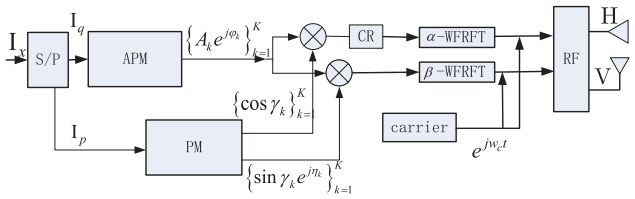

FIGURE 6. Block diagram of the transmitter.

Based on Eqs.(12) and (14), we obtain

$$\begin{aligned}\gamma_{\mathrm{R}k} &= \arctan\left(\frac{\mathrm{abs}\left(y_{\mathrm{V}k}\right)}{\mathrm{abs}\left(y_{\mathrm{H}k}\right)}\right) = \gamma_k,\\ \eta_{\mathrm{R}k} &= \Xi\left(y_{\mathrm{V}k}\right) - \Xi\left(y_{\mathrm{H}k}\right) = \eta_k - \theta_k.\end{aligned} \tag{28}$$

From Eq. (28), the phase difference is found to vary randomly, which lead to the PM constellation rotation. For the APM signal, based on Eq. (17), it can be obtained by

$$\begin{aligned}\mathbf{y}_k^{\mathrm{APM}} &= \begin{bmatrix}\cos\gamma_{\mathrm{R}k}\\ \sin\gamma_{\mathrm{R}k}e^{j\eta_{\mathrm{R}k}}\end{bmatrix}^{\mathrm{H}}\mathbf{y}_k\\ &= \sqrt{P\Upsilon}\begin{bmatrix}\cos\gamma_{\mathrm{R}k}\\ \sin\gamma_{\mathrm{R}k}e^{j\eta_{\mathrm{R}k}}\end{bmatrix}^{\mathrm{H}}\begin{bmatrix}\cos\gamma_k e^{j\theta_k}\\ \sin\gamma_k e^{j\eta_k}\end{bmatrix}A_k e^{j(w_c t+\varphi_k)}\\ &= \sqrt{P\Upsilon}A_k e^{j\theta_k}e^{j(w_c t+\varphi_k)}.\end{aligned} \tag{29}$$

From Eq. (29), the APM constellation is also found to be rotated randomly. In summary, the best choice is to multiply the pseudo random rotation angle with the horizontal component of the PM signal. In this way, both the PM and APM constellations are rotated randomly. Once the WFTFR signals are captured, the eavesdropper can not demodulate the signals accurately by scanning the WFRFT orders.

Finally, the block diagram of the transmitter is given in Fig. 6, the information sequence I_x is firstly divided into two sub-streams. Sub-stream I_q and sub-stream I_p are respectively processed by amplitude-phase modulation (APM) and polarization modulation (PM), which yield K APM symbols and K PM symbols. Subsequently, the k-th ($k = 1, 2, \cdots, K$) APM symbol is duplicated and multiplied with the two components of the k-th PM symbol, respectively. Then, we perform the pseudo random constellation rotation (CR) to the H component of the PM-APM signal. Later, the two components of the PM-APM signal are respectively processed by α-order and β-order 4WFRFT and then sent to the radio frequency (RF). Finally, the two components of the PM-APM signal are transmitted by H and V polarized antennas, respectively.

B. PDL EFFECT ELIMINATION

As analyzed in section III-B, the PDL effect will lead to the degradation of the demodulation performance of the authorized receiver. To solve the problem, we assume the CSI is estimated at the receiver side and a zero-forcing prefilter (ZFPF) [6] is applied before performing inverse WFRFT, which is equivalent to apply the filter

$$\mathbf{W} = \mathbf{G}^{-1} = \frac{\mathbf{G}^*}{\det(\mathbf{G})}, \tag{30}$$

where $\mathbf{G}$ denotes the estimated CSI and we assume $\mathbf{G} = \mathbf{H}$.

$$\mathbf{G}^* = \begin{bmatrix}h_{22} & -h_{12}\\ -h_{21} & h_{11}\end{bmatrix}. \tag{31}$$

As the channel estimation is not the main theme in this study, a perfect CSI is assumed to be obtained by the receivers. For both the authorized receiver Bob (B) and the eavesdropper Eve (E), the signals after filtering can be denoted as:

$$\begin{aligned}\tilde{\mathbf{y}}^{\mathrm{o}} &= \begin{bmatrix}\tilde{\mathbf{y}}_{\mathrm{H}}^{\mathrm{o}}\\ \tilde{\mathbf{y}}_{\mathrm{V}}^{\mathrm{o}}\end{bmatrix} = \sqrt{P}\mathbf{W}^{\mathrm{o}}\mathbf{H}^{\mathrm{o}}\begin{bmatrix}\Psi_4^{\alpha}\left(\mathbf{x}_{\mathrm{H}}^{\mathrm{r}}\right)\\ \Psi_4^{\beta}\left(\mathbf{x}_{\mathrm{V}}\right)\end{bmatrix} + \mathbf{W}^{\mathrm{o}}\begin{bmatrix}\mathbf{n}_{\mathrm{H}}^{\mathrm{o}}\\ \mathbf{n}_{\mathrm{V}}^{\mathrm{o}}\end{bmatrix}\\ &= \sqrt{P}\begin{bmatrix}\Psi_4^{\alpha}\left(\mathbf{x}_{\mathrm{H}}^{\mathrm{r}}\right)\\ \Psi_4^{\beta}\left(\mathbf{x}_{\mathrm{V}}\right)\end{bmatrix} + \begin{bmatrix}\tilde{\mathbf{n}}_{\mathrm{H}}^{\mathrm{o}}\\ \tilde{\mathbf{n}}_{\mathrm{V}}^{\mathrm{o}}\end{bmatrix},\end{aligned} \tag{32}$$

where $o = \mathrm{B}, \mathrm{E}$; $\mathbf{x}_{\mathrm{H}}^{\mathrm{r}}$ denotes the horizontal signal vector rotated by the pseudo random rotation angle; $\tilde{\mathbf{n}}_{\mathrm{H}}^{\mathrm{o}}$ and $\tilde{\mathbf{n}}_{\mathrm{V}}^{\mathrm{o}}$ are noise vectors, whose k-th elements can be represented as

$$\tilde{n}_{\mathrm{H}k}^{\mathrm{o}} = \frac{h_{22}^{\mathrm{o}}n_{\mathrm{H}k}^{\mathrm{o}} - h_{12}^{\mathrm{o}}n_{\mathrm{V}k}^{\mathrm{o}}}{\det(\mathbf{H}^{\mathrm{o}})}, \quad \tilde{n}_{\mathrm{V}k}^{\mathrm{o}} = \frac{h_{11}^{\mathrm{o}}n_{\mathrm{H}k}^{\mathrm{o}} - h_{21}^{\mathrm{o}}n_{\mathrm{V}k}^{\mathrm{o}}}{\det(\mathbf{H}^{\mathrm{o}})}. \tag{33}$$

It is easy to prove that the PDFs are [24]

$$\begin{aligned}\tilde{n}_{\mathrm{H}k}^{\mathrm{o}} &\sim \left(0, \frac{\left|h_{22}^{\mathrm{o}}\right|^2 + \left|h_{12}^{\mathrm{o}}\right|^2}{\det\left(\mathbf{H}^{\mathrm{o}}\right)^2}\sigma_{\mathrm{o}}^2\right),\\ \tilde{n}_{\mathrm{V}k}^{\mathrm{o}} &\sim \left(0, \frac{\left|h_{11}^{\mathrm{o}}\right|^2 + \left|h_{21}^{\mathrm{o}}\right|^2}{\det\left(\mathbf{H}^{\mathrm{o}}\right)^2}\sigma_{\mathrm{o}}^2\right).\end{aligned} \tag{34}$$

From Eq. (32), the PDL effect is found to be eliminated.

C. SECRECY CAPACITY PERFORMANCE ANALYSIS

In this section, the secrecy capacity performance of the CR-WFRFT scheme is evaluated. A more practical model is considered in which both the authorized receiver Bob and the eavesdropper Eve can accurately obtain the CSI, thus Eve can also apply the ZFPF method to eliminate the PDL effect.

For Bob, by using the parameters α and β, the signals after performing inverse WFRFT can be written as

$$\begin{aligned}\widehat{\mathbf{y}}^{\mathrm{B}} &= \begin{bmatrix}\widehat{\mathbf{y}}_{\mathrm{H}}^{\mathrm{B}}\\ \widehat{\mathbf{y}}_{\mathrm{V}}^{\mathrm{B}}\end{bmatrix} = \sqrt{P}\begin{bmatrix}\Psi_4^{-\alpha}\left(\Psi_4^{\alpha}\left(\mathbf{x}_{\mathrm{H}}^{\mathrm{r}}\right)\right)\\ \Psi_4^{-\beta}\left(\Psi_4^{\beta}\left(\mathbf{x}_{\mathrm{V}}\right)\right)\end{bmatrix} + \begin{bmatrix}\Psi_4^{-\alpha}\left(\tilde{\mathbf{n}}_{\mathrm{H}}^{\mathrm{B}}\right)\\ \Psi_4^{-\beta}\left(\tilde{\mathbf{n}}_{\mathrm{V}}^{\mathrm{B}}\right)\end{bmatrix}\\ &= \sqrt{P}\begin{bmatrix}\mathbf{x}_{\mathrm{H}}^{\mathrm{r}}\\ \mathbf{x}_{\mathrm{V}}\end{bmatrix} + \begin{bmatrix}\widehat{\mathbf{n}}_{\mathrm{H}}^{\mathrm{B}}\\ \widehat{\mathbf{n}}_{\mathrm{V}}^{\mathrm{B}}\end{bmatrix},\end{aligned} \tag{35}$$

where $\widehat{\mathbf{n}}_{\mathrm{H}}^{\mathrm{B}}$ ($\widehat{\mathbf{n}}_{\mathrm{V}}^{\mathrm{B}}$) is the noise vector processed by the inverse WFRFT, whose PDF is the same as $\tilde{\mathbf{n}}_{\mathrm{H}}^{\mathrm{B}}$ ($\tilde{\mathbf{n}}_{\mathrm{V}}^{\mathrm{B}}$) for WFRFT is a kind of unitary transformation. Then, by using the pseudo random rotation angle vector $\mathbf{R} = \left[e^{j\theta_1}, e^{j\theta_2}, \cdots, e^{j\theta_K}\right]^{\mathrm{H}}$, the

inverse constellation rotation (ICR) can be performed to $\widehat{\mathbf{y}}_{\mathrm{H}}^{\mathrm{B}}$ to produce

$$\mathbf{y}_{\mathrm{R}}^{\mathrm{B}} = \begin{bmatrix} \mathbf{y}_{\mathrm{HR}}^{\mathrm{B}} \\ \mathbf{y}_{\mathrm{VR}}^{\mathrm{B}} \end{bmatrix} = \sqrt{P}\begin{bmatrix} \mathbf{x}_{\mathrm{H}}^{\mathrm{r}}\mathbf{R} \\ \mathbf{x}_{\mathrm{V}} \end{bmatrix} + \begin{bmatrix} \widehat{\mathbf{n}}_{\mathrm{H}}^{\mathrm{B}}\mathbf{R} \\ \widehat{\mathbf{n}}_{\mathrm{V}}^{\mathrm{B}} \end{bmatrix} = \sqrt{P}\begin{bmatrix} \mathbf{x}_{\mathrm{H}} \\ \mathbf{x}_{\mathrm{V}} \end{bmatrix} + \begin{bmatrix} \breve{\mathbf{n}}_{\mathrm{H}}^{\mathrm{B}} \\ \widehat{\mathbf{n}}_{\mathrm{V}}^{\mathrm{B}} \end{bmatrix}, \tag{36}$$

where $\breve{\mathbf{n}}_{\mathrm{H}}^{\mathrm{B}} = \widehat{\mathbf{n}}_{\mathrm{H}}^{\mathrm{B}}\mathbf{R}$. Finally, based on the demodulation method illustrated in section III-B, the information can be recovered. From Eq. (36), for each symbol, the SNR can be calculated by

$$\xi_{\mathrm{B}k} = P\frac{|\mathbf{x}_{\mathrm{H}}(k)|^2 + |\mathbf{x}_{\mathrm{V}}(k)|^2}{\left|\breve{\mathbf{n}}_{\mathrm{H}}^{\mathrm{B}}(k)\right|^2 + \left|\widehat{\mathbf{n}}_{\mathrm{V}}^{\mathrm{B}}(k)\right|^2} = \frac{PA_k \det(\mathbf{H}^{\mathrm{B}})^2}{\left(\left|h_{22}^{\mathrm{B}}\right|^2 + \left|h_{12}^{\mathrm{B}}\right|^2 + \left|h_{11}^{\mathrm{B}}\right|^2 + \left|h_{21}^{\mathrm{B}}\right|^2\right)\sigma_{\mathrm{B}}^2}. \tag{37}$$

For the eavesdropper Eve, the signals after performing inverse WFRFT can be written as

$$\widehat{\mathbf{y}}^{\mathrm{E}} = \begin{bmatrix} \widehat{\mathbf{y}}_{\mathrm{H}}^{\mathrm{E}} \\ \widehat{\mathbf{y}}_{\mathrm{V}}^{\mathrm{E}} \end{bmatrix} = \sqrt{P}\begin{bmatrix} \Psi_4^{\alpha_1}\left(\Psi_4^{\alpha}\left(\mathbf{x}_{\mathrm{H}}^{\mathrm{r}}\right)\right) \\ \Psi_4^{\beta_1}\left(\Psi_4^{\beta}\left(\mathbf{x}_{\mathrm{V}}\right)\right) \end{bmatrix} + \begin{bmatrix} \Psi_4^{\alpha_1}\left(\tilde{\mathbf{n}}_{\mathrm{H}}^{\mathrm{E}}\right) \\ \Psi_4^{\beta_1}\left(\tilde{\mathbf{n}}_{\mathrm{V}}^{\mathrm{E}}\right) \end{bmatrix} = \sqrt{P}\begin{bmatrix} \Psi_4^{\Delta\alpha}\left(\mathbf{x}_{\mathrm{H}}^{\mathrm{r}}\right) \\ \Psi_4^{\Delta\beta}\left(\mathbf{x}_{\mathrm{V}}\right) \end{bmatrix} + \begin{bmatrix} \Psi_4^{\alpha_1}\left(\tilde{\mathbf{n}}_{\mathrm{H}}^{\mathrm{E}}\right) \\ \Psi_4^{\beta_1}\left(\tilde{\mathbf{n}}_{\mathrm{V}}^{\mathrm{E}}\right) \end{bmatrix}. \tag{38}$$

As analyzed in section IV-A, after pseudo randomly rotating the constellations, Eve can not accurately obtain the orders α and β, thus $\Delta\alpha > 0$, $\Delta\beta > 0$. According to Eq. (7), the signals after performing inverse WFRFT can be further written as

$$\begin{bmatrix} \Psi_4^{\Delta\alpha}\left(\mathbf{x}_{\mathrm{H}}^{\mathrm{r}}\right) \\ \Psi_4^{\Delta\beta}\left(\mathbf{x}_{\mathrm{V}}\right) \end{bmatrix} = \begin{bmatrix} \mathbf{W}_4^{\Delta a}\left(\mathbf{x}_{\mathrm{H}}^{\mathrm{r}}\right)^{\mathrm{T}} \\ \mathbf{W}_4^{\Delta\beta}\left(\mathbf{x}_{\mathrm{V}}\right)^{\mathrm{T}} \end{bmatrix} = \begin{bmatrix} \underbrace{w_0(\Delta a)\left(\mathbf{x}_{\mathrm{H}}^{\mathrm{r}}\right)^{\mathrm{T}}}_{\text{Useful }(\mathbf{f}_{\mathrm{HU}})} + \underbrace{\begin{pmatrix} w_1(\Delta a)\mathbf{F}_K\left(\mathbf{x}_{\mathrm{H}}^{\mathrm{r}}\right)^{\mathrm{T}} \\ +w_2(\Delta a)\mathbf{P}_K\left(\mathbf{x}_{\mathrm{H}}^{\mathrm{r}}\right)^{\mathrm{T}} \\ +w_3(\Delta a)\mathbf{P}\mathbf{F}_K\left(\mathbf{x}_{\mathrm{H}}^{\mathrm{r}}\right)^{\mathrm{T}} \end{pmatrix}}_{\text{self - Interference}(\mathbf{f}_{\mathrm{HI}})} \\ \underbrace{w_0(\Delta\beta)\left(\mathbf{x}_{\mathrm{V}}\right)^{\mathrm{T}}}_{\text{Useful}(\mathbf{f}_{\mathrm{VU}})} + \underbrace{\begin{pmatrix} w_1(\Delta\beta)\mathbf{F}_K\left(\mathbf{x}_{\mathrm{V}}\right)^{\mathrm{T}} \\ +w_2(\Delta\beta)\mathbf{P}_K\left(\mathbf{x}_{\mathrm{V}}\right)^{\mathrm{T}} \\ +w_3(\Delta\beta)\mathbf{P}\mathbf{F}_K\left(\mathbf{x}_{\mathrm{V}}\right)^{\mathrm{T}} \end{pmatrix}}_{\text{self - Interference}(\mathbf{f}_{\mathrm{VI}})} \end{bmatrix}. \tag{39}$$

From Eq. (39), it is found that only the first parts ($\mathbf{f}_{\mathrm{HU}}$ and $\mathbf{f}_{\mathrm{VU}}$) are useful, which can be used for further processing, i.e., inverse rotation. The other three parts ($\mathbf{f}_{\mathrm{HI}}$ and $\mathbf{f}_{\mathrm{VI}}$) are useless and treated as self-interferences. In addition, constellation rotation does not change the signal's power and, thus for each symbol, the SNR of Eve is calculated as

$$\begin{aligned} \xi_{\mathrm{E}k} &= \frac{P\left(|\mathbf{f}_{\mathrm{HU}}(k)|^2 + |\mathbf{f}_{\mathrm{VU}}(k)|^2\right)}{P\left(|\mathbf{f}_{\mathrm{HI}}(k)|^2 + |\mathbf{f}_{\mathrm{VI}}(k)|^2\right) + \left|\widehat{\mathbf{n}}_{\mathrm{H}}^{\mathrm{E}}(k)\right|^2 + \left|\widehat{\mathbf{n}}_{\mathrm{V}}^{\mathrm{E}}(k)\right|^2} \\ &= \frac{P\left(|\mathbf{f}_{\mathrm{HU}}(k)|^2 + |\mathbf{f}_{\mathrm{VU}}(k)|^2\right)\det(\mathbf{H}^{\mathrm{E}})^2}{P\det(\mathbf{H}^{\mathrm{E}})^2\left(|\mathbf{f}_{\mathrm{HI}}(k)|^2 + |\mathbf{f}_{\mathrm{VI}}(k)|^2\right) + \left(\begin{matrix}\left|h_{22}^{\mathrm{E}}\right|^2 + \left|h_{12}^{\mathrm{E}}\right|^2 \\ + \left|h_{11}^{\mathrm{E}}\right|^2 + \left|h_{21}^{\mathrm{E}}\right|^2\end{matrix}\right)\sigma_{\mathrm{E}}^2} \\ &= \frac{PA_k^2\left(|w_0(\Delta a)\cos\gamma_k|^2 + |w_0(\Delta\beta)\sin\gamma_k|^2\right)\det(\mathbf{H}^{\mathrm{E}})^2}{\left(\begin{matrix} PA_k^2\det(\mathbf{H}^{\mathrm{E}})^2\left(\begin{matrix}2 - |w_0(\Delta a)\cos\gamma_k|^2 \\ -|w_0(\Delta\beta)\sin\gamma_k|^2\end{matrix}\right) \\ + \left(\left|h_{22}^{\mathrm{E}}\right|^2 + \left|h_{12}^{\mathrm{E}}\right|^2 + \left|h_{11}^{\mathrm{E}}\right|^2 + \left|h_{21}^{\mathrm{E}}\right|^2\right)\sigma_{\mathrm{E}}^2 \end{matrix}\right)}. \end{aligned} \tag{40}$$

The secrecy capacity is the bit rate at which Bob can recover the information, while Eve cannot recover the information accurately. Therefore, a larger secrecy capacity guarantees a more security performance. According to [25], in the Gauss wiretap channel, the secrecy capacity is the difference between the capacity of Bob and Eve. In the present system, the average secrecy capacity difference of Bob and Eve is considered as

$$C_{\mathrm{ave}} = \mathop{\mathrm{E}}_{\mathbf{H}_{\mathrm{B}},\mathbf{H}_{\mathrm{E}}}\left[\frac{10}{K}\sum_{k=1}^{K}\log_{10}\frac{1+\xi_{\mathrm{B}k}}{1+\xi_{\mathrm{E}k}}\right]. \tag{41}$$

From Eqs. (37) and (40), $\xi_{\mathrm{B}k}$ is found to be mainly affected by the noise, while $\xi_{\mathrm{E}k}$ is affected by both the noise and self-interferences. As the eavesdropper cannot obtain the WFRFT orders accurately, the self-interferences cannot be eliminated. Therefore, a positive secrecy capacity is always achieved in the CR-WFRFT scheme.

D. STATISTICAL CSI BASED ANALYSIS

To evaluate the effects of noise on the capacity, it would be a good choice to employ the statistical channel state information (CSI) since the coherent time of the statistical CSI is much longer than the instantaneous CSI [26]. Then, the 2×2 satellite channel impulse response matrix $\mathbf{H}$ is denoted as

$$\mathbf{H}^{\mathrm{o}} = \sqrt{\frac{K}{K+1}}\bar{\mathbf{H}}^{\mathrm{o}} + \sqrt{\frac{1}{K+1}}\tilde{\mathbf{H}}^{\mathrm{o}}, \quad \mathrm{o} = \mathrm{B,E}. \tag{42}$$

where $\bar{\mathbf{H}}^{\mathrm{o}}$ denotes the line of sight (LOS) component, $\tilde{\mathbf{H}}^{\mathrm{o}}$ the non-LOS component and K^{o} the Rice factor [4]. Then, we can obtain

$$\begin{aligned} \mathrm{E}\left[\mathbf{H}^{\mathrm{o}}\right] &= \sqrt{\frac{K^{\mathrm{o}}}{K^{\mathrm{o}}+1}}\mathrm{E}\left[\bar{\mathbf{H}}^{\mathrm{o}}\right] + \sqrt{\frac{1}{K^{\mathrm{o}}+1}}\mathrm{E}\left[\tilde{\mathbf{H}}^{\mathrm{o}}\right] \\ &= \sqrt{\frac{K^{\mathrm{o}}}{K^{\mathrm{o}}+1}}\bar{\mathbf{H}}^{\mathrm{o}} = \sqrt{\frac{K^{\mathrm{o}}\Upsilon}{K^{\mathrm{o}}+1}}\begin{bmatrix}\sqrt{1-\beta^{\mathrm{o}}} & \sqrt{\beta^{\mathrm{o}}} \\ \sqrt{\beta^{\mathrm{o}}} & \sqrt{1-\beta^{\mathrm{o}}}\end{bmatrix}, \end{aligned}$$

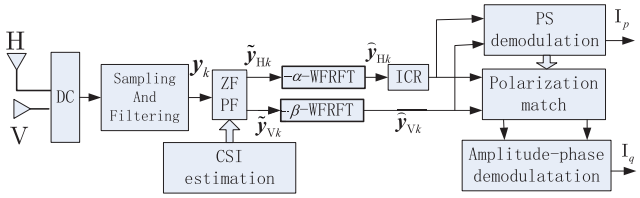

FIGURE 7. Block diagram of the receiver designed for Bob.

(43)

where $\mathrm{E}[\bullet]$ denotes the expectation acquisition function; β^{o} is the parameter characterising the XPD of the antennas, which is calculated by

$$\zeta^{\mathrm{o}} = 10\log_{10}\left(\frac{1-\beta^{\mathrm{o}}}{\beta^{\mathrm{o}}}\right). \tag{44}$$

Based on Eq. (43), derivation yields

$$\frac{\left|h_{22}^{\mathrm{o}}\right|^2+\left|h_{12}^{\mathrm{o}}\right|^2+\left|h_{11}^{\mathrm{o}}\right|^2+\left|h_{21}^{\mathrm{o}}\right|^2}{\det\left(\mathbf{H}^{\mathrm{o}}\right)^2} = \frac{2\left(1+K^{\mathrm{o}}\right)}{\left(1-2\beta^{\mathrm{o}}\right)^2 K^{\mathrm{o}}\Upsilon}. \tag{45}$$

Based on Eq. (45), Eqs.(37) and (40) can be simplified to

$$\xi_{\mathrm{B}k} = \frac{PA_k^2\left(1-2\beta^{\mathrm{B}}\right)^2 K^{\mathrm{B}}\Upsilon}{2\left(1+K^{\mathrm{B}}\right)\sigma_{\mathrm{B}}^2}, \tag{46}$$

$$s\xi_{\mathrm{E}k} = \frac{PA_k^2\left(\left|w_0\left(\Delta a\right)\cos\gamma_k\right|^2+\left|w_0\left(\Delta\beta\right)\sin\gamma_k\right|^2\right)}{\left(\begin{array}{l}PA_k^2\left(2-\left|w_0(\Delta a)\cos\gamma_k\right|^2-\left|w_0(\Delta\beta)\sin\gamma_k\right|^2\right)\\+\frac{2\left(1+K^{\mathrm{E}}\right)}{\left(1-2\beta^{\mathrm{E}}\right)^2 K^{\mathrm{E}}\Upsilon}\sigma_{\mathrm{E}}^2\end{array}\right)}. \tag{47}$$

From Eq. (46) and Eq. (47), it is found that the SNR of both Bob and Eve are affected by the XPD of the receiver antenna and a smaller XPD will lead to a relatively larger attenuation in the SNR, which will deteriorate the demodulation performance. In the next section, the theoretical analysis will be demonstrated by the simulation results.

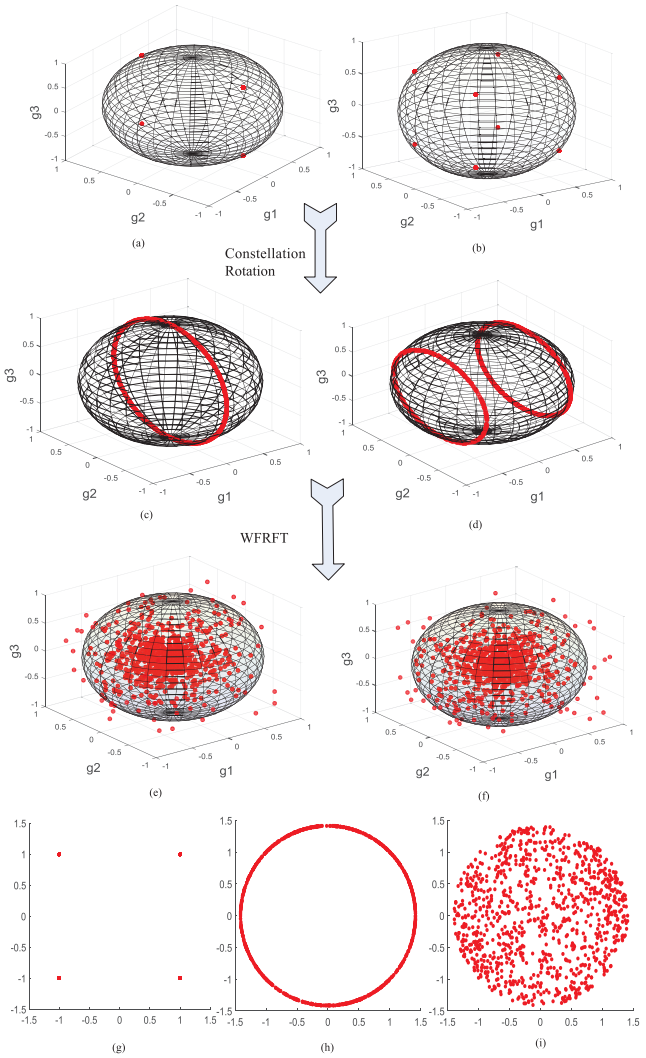

FIGURE 8. Constellation distortion pattern after constellation rotation and WFRFT. The original constellation points are shown by (a), (b), and (g). After constellation rotation, the constellation points are shown by (c), (d), and (h). After processed by WFRFT, the constellation points are shown by (e), (f), and (i). The parameters are ($\zeta^{\mathrm{o}} = \infty$, $\alpha = \beta = 0.7$, $M_p = 4$, $M_q = 4$).

V. SIMULATION RESULTS

In the CR-WFRFT scheme, the transmitter designed for Alice is shown in Fig. 6 and the block diagram of the receiver designed for Bob is shown in Fig. 7.

In Fig. 7, the ZFPF method is used to eliminate the PDL effect after down convention (DC), sampling and filtering. Then, the inverse WFRFT operations are performed. After performing inverse constellation rotation (ICR) to the H component, signals can be demodulated based on the method mentioned in III-A. To evaluate the security performance of the CR-WFRFT scheme, four simulations are described below.

A. CONSTELLATION DISTORTION

In the CR-WFRFT scheme, the H components of the PM-APM signal are firstly rotated by the pseudo random rotation angles and then both the H and V components are processed by WFRFT. Fig. 8 shows the constellation distortion patterns of the 4PM, 8PM and the QPSK constellations after processed by constellation rotation (CR) and WFRFT, where 1024 symbols are randomly generated for simulations. It is found that after constellation rotation, both the PM and QPSK constellation points are randomly distributed over the circumference, which prove the effectiveness of the constellation rotation method proposed in section IV-A. Then, after processing by WFRFT, the PM signals are randomly distributed in, on, and outside the sphere and the QPSK signals are randomly distributed on a circular surface. As discussed in Fig. 4, by appropriately selecting the WFRFT orders, the distribution of the WFRFT signals is nearly Gaussian, thus the signals are difficult to detect. Moreover, the eavesdropper can only obtain the randomly rotated signals through the

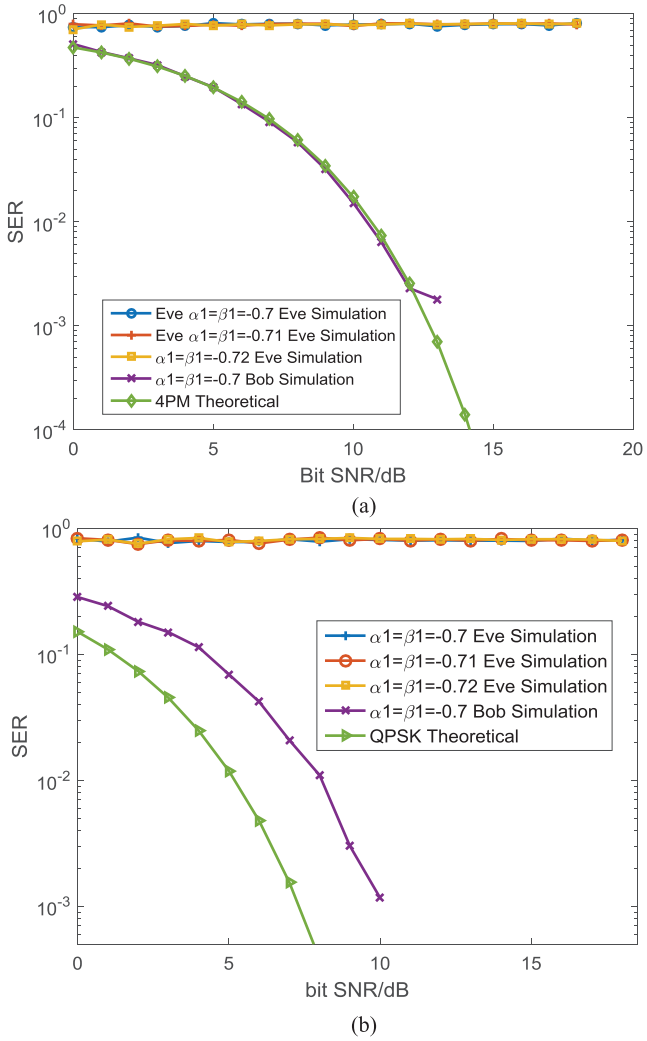

FIGURE 9. Anti-scanning performance of the CR-WFRFT scheme. The parameters are ($\zeta^{o} = \infty$, $\alpha = \beta = 0.7$, $M_p = M_q = 4$, $K = \infty$). (a) Anti-scanning performance of the 4PM signal. (b) Anti-scanning performance of the QPSK signal.

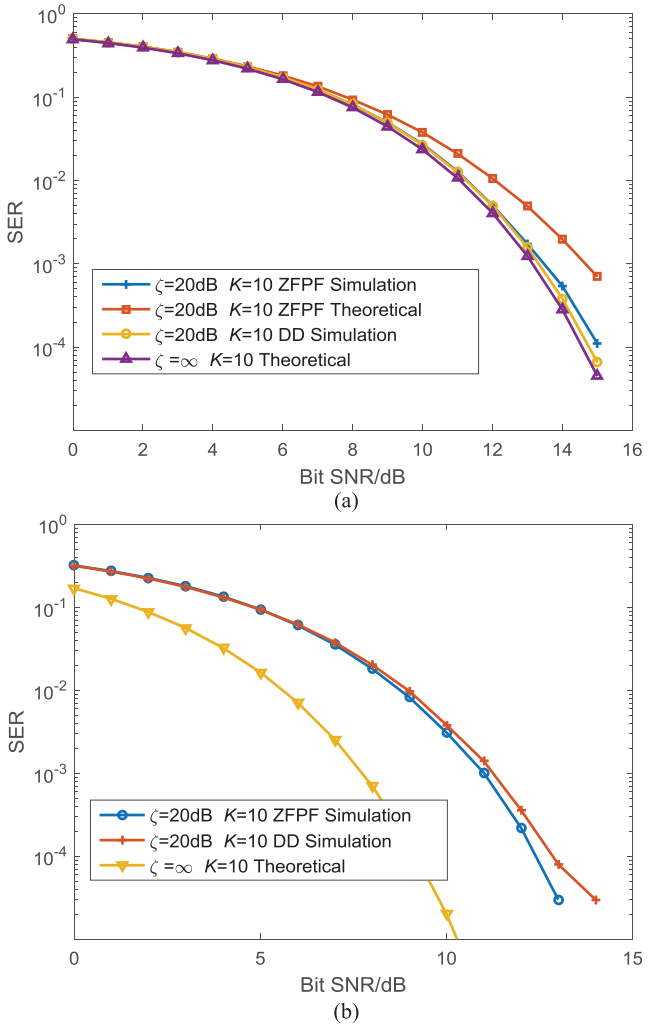

FIGURE 10. SER curves of different demodulation methods versus Bit SNR under non-ideal channel conditions. The parameters are ($M_p = 4$, $M_q = 4$, $\alpha = \beta = 0.7$). (a) SER performance of PM. (b) SER performance of APM.

parameter scanning method, thus the WFRFT orders are also difficult to be cracked, which further causes self-interferences at the eavesdropper side.

B. ANTI-SCANNING PERFORMANCE OF THE CR-WFRFT SCHEME

In this section, the anti-scanning performance of the CR-WFRFT scheme is demonstrated in terms of the symbol error rate (SER). An ideal channel condition is assumed and the eavesdropper is assumed to have the information of the modulation techniques and the modulation orders, but do not know the pseudo random rotation angles. QPSK and 4PM are used to form the PM-APM signal.

Fig. 9 shows the anti-scanning performance of the CR-WFRFT scheme under different scan error conditions. It is found that for Bob, the SER performance of the PM signal is almost the same as the theoretical values (the theoretical SER is calculated based on the calculations in the Appendix). For APM signals, the SER performance is a little worse than the theoretical values because of the non-ideal polarization matching. For Eve, even with an ideal channel condition and small scanning errors, i.e., $\Delta\alpha = \Delta\beta \in \{0, 0.1, 0.2\}$, the SER curves are still high, which means that it is difficult to demodulate the WFRFT signals through the order scanning method and, thus good protection is offered and the transmission security is enhanced by the CR-WFRFT scheme.

C. SER PERFORMANCE UNDER THE NON-IDEAL CHANNEL CONDITIONS

As shown in Fig. 9, under the ideal channel condition, the SER of Eve is high. Thus, in this section, only the SER of Bob is observed under the non-ideal channel condition. Fig. 10 plots the SER curves of different PDL elimination methods. In Fig. 10(a), the SER performance of 4PM signal is given, where the theoretical value can be calculated by the method in the Appendix and the symbol SNR can be calculated based

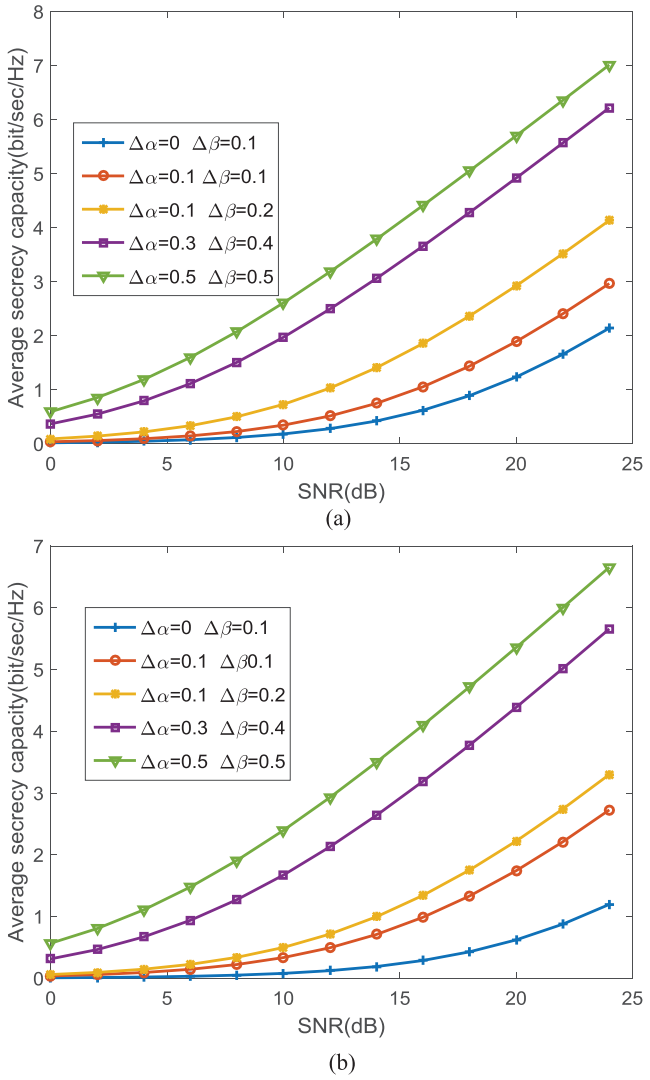

FIGURE 11. Average secrecy capacity performance versus SNR with different scanning errors. The parameters are ($\alpha = \beta = 0.7$,$K = 10$, ζ=23 dB). (a) Average secrecy capacity versus SNR. The parameters are ($M_P = 4$, $M_q = 4$). (b) Average secrecy capacity versus SNR. The parameters are ($M_P = 8$, $M_q = 16$).

on Eq. (46). It is found that the SER performance of the ZFPF method is closer to the theoretical value than that of the direct demodulation (DD) method based on Eq. (14)-(16). This is because the PDL is eliminated with the ZFPF method. In addition, the SER performance of the ZFPF method is a little worse than the theoretical value. This is mainly due to the SNR degradation caused by the non-ideal XPD, as shown by Eq. (46).

Fig. 10(b) shows the SER performance of the QPSK signal. The theoretical value is obtained under the Gauss channel with $K = 10$, which is calculated by Eq. (22), where $\xi = \xi_k^{\mathrm{B}}$. It is found that the SER performance of both the ZFPF method and the DD method are worse than the theoretical value. This is mainly because in the CR-WFRFT scheme, the demodulation of the QPSK signal is affected by the polarization match and in the low SNR condition, affected by noise, the correct demodulation probability (CDP) of the signal's PS is low. Moreover, the SER performance of the ZFPF method is a little better than that of the DD method and this is because the CDP of the signal's PS with the ZFPF method is higher than that with the DD method.

D. SECRECY CAPACITY PERFORMANCE OF THE CR-WFRFT SCHEME

Fig. 11 shows the average secrecy capacity performance versus SNR with different scanning errors. Fig. 11(a) shows the average secrecy capacity performance of the PM-APM signal consisting of 4PM and QPSK. Fig. 11(b) shows the average secrecy capacity performance of the PM-APM signal consisting of 8PM and 16QAM. It is found that the average secrecy capacity increases as $\Delta\alpha$ and $\Delta\beta$ increases. Moreover, the average secrecy capacity also monotonically increases with SNR. In the CR-WFRFT scheme, for the eavesdropper, scanning errors are inevitable due to the constellation rotation. Therefore, a positive secret rate can always be achieved and chosen for further enhancing the transmission security.

VI. CONCLUSION

In this paper, we propose a CR-WFRFT scheme to enhance the physical layer security in dual-polarized satellite communication. Based on the constellation rotation method, both the PM and APM constellations are randomly rotated, which make it hard for the eavesdropper to crack the WFRFT orders through the WFRFT order scanning method. Moreover, the scanning errors in WFRFT order will bring self-interferences at the eavesdropper side, thus the SNR will decrease. In this way, a positive average secret capacity can be achieved and chosen for further enhancing the transmission security. Even the eavesdropper has the information regarding the modulation techniques and modulation order, it is still impossible to demodulate the signal with the proposed scheme.

APPENDIX

In this appendix, we give the calculation method of the theoretical value of the symbol error rate (SER) of PM signals under Gauss channel. The constellation is shown in Fig. 3. To derive the SER, the maximum likelihood decision model is established as

$$\hat{\mathbf{P}}_k = \min_{1 \le m \le M} \mathrm{dis}\left(\mathbf{P}_{\mathrm{R}k}, \mathbf{P}_{\mathrm{T}m}\right), \tag{48}$$

where $\mathbf{P}_{\mathrm{T}m}$ is the transmitted polarization constellation point and $\mathbf{P}_{\mathrm{R}k}$ is the k-th received signal. dis $(\mathbf{P}_Z, \mathbf{P}_B)$ denotes the sphere distance between $\mathbf{P}_Z$ and $\mathbf{P}_B$. Affected by the noise, $\mathbf{P}_{\mathrm{R}k}$ will deviate from the transmitted PS. Then, under the disturbance of the noise, the joint probability density function of $\mathbf{P}_{\mathrm{R}k}$'s co-latitude t_i and azimuth φ_i can be denoted as

$$f\left(t_i, \varphi_i\right) = \frac{\sin t_i}{4\pi} e^{-\xi(1-\cos t_i)/2}\left[1 + \xi(1+\cos t_i)/2\right], \tag{49}$$

where ξ denotes the symbol SNR. Then the SER can be derived by Eq. (50)- Eq. (54)

$$S_{er} = \frac{1}{M_p}\sum_{i=1}^{M_p} g_i, \tag{50}$$

$$g_i = \begin{cases} \left[\int_{\pi-\vartheta_0}^{\pi}\int_{0}^{2\pi} f(t_i,\varphi_i)\,\mathrm{d}\varphi_i\mathrm{d}t_i + \int_{\vartheta_0}^{\pi-\vartheta_0}\int_{0}^{\alpha(\vartheta_0,t_i)} f(t_i,\varphi_i)\,\mathrm{d}\varphi_i\mathrm{d}t_i\right] \\ \quad \left(M_p=2\right), \\ \sum_{j=1}^{c} 2\left[\int_{\psi_{ij}}^{\pi}\int_{0}^{\alpha(\vartheta_0,\psi_{ij})} f(t_i,\varphi_i)\,\mathrm{d}\varphi_i\mathrm{d}t_i + \int_{\vartheta_0}^{\psi_{ij}}\int_{0}^{\alpha(\vartheta_0,t_i)} f(t_i,\varphi_i)\,\mathrm{d}\varphi_i\mathrm{d}t_i\right] \\ \quad \left(M_p>2\right). \end{cases} \tag{51}$$

$$\alpha(\vartheta_0,t_i) = \arccos(tan\vartheta_0/t_i),\ \vartheta_0 = d_{\mathrm{T}}, \tag{52}$$

where ψ_{ij} denotes the sphere distance between $\mathbf{P}_{\mathrm{Rk}}$ and the endpoints of its decision region (c is the number of endpoints) as

$$\begin{cases} \psi_{i1} = 2\gamma_{\mathrm{R}}^{i}, \quad \psi_{i2} = \pi - 2\gamma_{\mathrm{R}}^{i}, \quad \left(M_p=4;\, i\in[1,4]\right);\ k=2 \\ \psi_{i1} = \psi_{i2} = \arccos\left[\dfrac{\cos 2\gamma_{\mathrm{R}}^{i}+\sin 2\gamma_{\mathrm{R}}^{i}\tan\left(\gamma_{\mathrm{R}}^{i}+\gamma_{\mathrm{R}}^{i+M/2}\right)}{1+\sec^2(O/2)\tan^2\left(\gamma_{\mathrm{R}}^{i}+\gamma_{\mathrm{R}}^{i+M/2}\right)}\right] \\ \psi_{i3} = 2\gamma_{\mathrm{R}}^{i}, \quad \left(M_p\geq 8;\, i\in\left[1,M_p/2\right]\right);\ k=3 \\ \psi_{i1} = \psi_{i2} = arc\cos\left[\dfrac{\cos\left(\gamma_{\mathrm{R}}^{i}-\gamma_{\mathrm{R}}^{i-M/2}\right)}{1+\sin^2\left(\gamma_{\mathrm{R}}^{i}+\gamma_{\mathrm{R}}^{i+M/2}\right)\tan^2(O/2)}\right] \\ \psi_{i3} = \pi - 2\gamma_{\mathrm{R}}^{i}, \quad \left(M_p\geq 8;\, i\in\left[1,M_p/2\right]\right);\ k=3 \end{cases} \tag{53}$$

where O is the spheric angle between the adjacent polarization constellation points as

$$O = \angle\mathbf{P}_{\mathrm{R}i}\mathbf{P}_{\mathrm{H}}\mathbf{P}_{\mathrm{R}j} = 2\arcsin\left[\sin(\vartheta_0)/\sin(2\gamma_i)\right]. \tag{54}$$

REFERENCES

[1] P.-D. Arapoglou, K. Liolis, M. Bertinelli, A. Panagopoulos, P. Cottis, and R. de Gaudenzi, "Mimo over satellite: A review," *IEEE Commun. Surv. Tut.*, vol. 13, no. 1, pp. 27–51, 1st Quart., 2011.
[2] M. Yofune, J. Webber, K. Yano, H. Ban, and K. Kobayashi, "Optimization of signal design for poly-polarization multiplexing in satellite communications," *IEEE Commun. Lett.*, vol. 17, no. 11, pp. 2017–2020, Nov. 2013.
[3] P.-D. Arapoglou, P. Burzigotti, M. Bertinelli, A. B. Alamanac, and R. de Gaudenzi, "To MIMO or not to MIMO in mobile satellite broadcasting systems," *IEEE Trans. Wireless Commun.*, vol. 10, no. 9, pp. 2807–2811, Sep. 2011.
[4] K. P. Liolis, J. Gomez-Vilardebo, E. Casini, and A. I. Pérez-Neira, "Statistical modeling of dual-polarized MIMO land mobile satellite channels," *IEEE Trans. Commun.*, vol. 58, no. 11, pp. 3077–3083, Nov. 2010.
[5] V. Nikolaidis, N. Moraitis, and A. G. Kanatas, "Dual-polarized narrowband MIMO LMS channel measurements in urban environments," *IEEE Trans. Antenn. Propag.*, vol. 65, no. 2, pp. 763–774, Feb. 2017.
[6] P. Henarejos and A. I. Pérez-Neira, "Dual polarized modulation and reception for next generation mobile satellite communications," *IEEE Trans. Commun.*, vol. 63, no. 10, pp. 3803–3812, Oct. 2015.
[7] L. J. Arend, "On dual-polarization signalling techniques in satellite communications," M.S. thesis, Univ. Luxembourg, Esch-sur-Alzettel, Luxembourg, 2015.
[8] L. Arend, R. Sperber, M. Marso, and J. Krause, "Implementing polarization shift keying over satellite—System design and measurement results," *Int. J. Satell. Commun. Netw.*, vol. 34, no. 2, pp. 211–229, Mar./Apr. 2016.
[9] Z. Luo, H. Wang, and W. Lv, "Directional polarization modulation for secure transmission in dual-polarized satellite MIMO systems," in *Proc. IEEE 8th Int. Conf. Wireless Commun. Signal Process.*, Yangzhou China, Oct. 2016, pp. 1–5.
[10] W. Dong, Z. Meng, F. Wei, and H. Weiqing, "A spectrum efficient polarized PSK/QAM scheme in the wireless channel with polarization dependent loss effect," in *Proc. IEEE Int. Conf. Telecommun.*, Sydney, NSW, Australia, Apr. 2015, pp. 249–255.
[11] D. Wei, C. Feng, C. Guo, and L. Fangfang, "A power amplifier energy efficient polarization modulation scheme based on the optimal precompensation," *IEEE Commun. Lett.*, vol. 17, no. 3, pp. 513–516, Mar. 2013.
[12] W. Dong, F. Chunyan, and G. Caili, "An optimal pre-compensation based joint polarization-amplitude-phase modulation scheme for the power amplifier energy efficiency improvement," in *Proc. IEEE Int. Conf. Commun.*, Budapest, Hungary, Jun. 2013, pp. 4137–4142.
[13] Z. Gan, P.-D. Arapoglou, and B. Ottersten, "Physical layer security in multibeam satellite systems," *IEEE Trans. Wireless Commun.*, vol. 11, no. 2, pp. 852–863, Feb. 2012.
[14] D. Shan, K. Zeng, W. Xiang, P. Richardson, and Y. Dong, "PHY-CRAM: Physical layer challenge-response authentication mechanism for wireless networks," *IEEE J. Sel. Areas Commun.*, vol. 31, no. 9, pp. 1817–1827, Sep. 2013.
[15] E. Jorswieck, S. Tomasin, and A. Sezgin, "Broadcasting into the uncertainty: Authentication and confidentiality by physical-layer processing," *Proc. IEEE*, vol. 103, no. 10, pp. 1702–1724, Oct. 2015.
[16] W. Trappe, "The challenges facing physical layer security," *IEEE Commun. Mag.*, vol. 53, no. 6, pp. 16–20, Jun. 2015.
[17] L. Mei, X. Sha, Q. Ran, and N. Zhang, "Research on the application of 4-weighted fractional fourier transform in communication system," *Sci. China Inf. Sci.*, vol. 53, no. 6, pp. 1251–1260, Jun. 2010.
[18] X. Fang, X. Wu, N. Zhang, X. Sha, and X. Shen, "Safeguarding physical layer security using weighted fractional fourier transform," in *Proc. IEEE Int. Conf. Global Commun.*, Washington, DC, USA, Dec. 2016, pp. 1–6.
[19] L. Mei, X.-J. Sha, and N.-T. Zhang, "The approach to carrier scheme convergence based on 4-weighted fractional fourier transform," *IEEE Commun. Lett.*, vol. 14, no. 6, pp. 503–505, Jun. 2010.
[20] Z. Luo, H. Wang, and K. Zhou, "Physical layer security scheme based on polarization modulation and WFRFT processing for dual-polarized satellite systems," *KSII Trans. Internet Inf.*, to be published.
[21] X. Fang, N. Zhang, X. Sha, D. Chen, X. Wu, and X. S. Shen, "Physical layer security: A WFRFT-basec cooperation approach," in *Proc. IEEE Int. Conf. Commun.*, May 2017, pp. 1–6.
[22] B. Ding, M. Lin, and X. Sha, "Secure communication system based on alterable-parameter 4-weighted," *Inf. Technol. J.*, vol. 9, no. 1, pp. 158–163, Jan. 2010.
[23] R. Ma, L. Dai, Z. Wang, and J. Wang, "Secure communication in TDS-OFDM system using constellation rotation and noise insertion," *IEEE Trans. Consum. Electron.*, vol. 56, no. 3, pp. 1328–1332, Aug. 2010.
[24] Y. Yang, X. Xin, J. Bin, and G. Xiqi, "An adaptive coding method for dual-polarized mobile satellite communications," in *Proc. IEEE Int. Conf. Wireless Commun. Signal Process.*, Hefei, China, Oct. 2013, pp. 1–5.
[25] A. D. Wyner, "The wire-tap channel," *Bell Syst. Tech. J.*, vol. 54, no. 8, pp. 1355–1387, Oct. 1975.
[26] T. Qi and Y. Wang, "Capacity analysis of a land mobile satellite system using dual-polarized antennas for diversity," in *Proc. IEEE 82nd Veh. Tech. Conf.*, Boston, MA, USA, Sep. 2016, pp. 1–5.

ZHANGKAI LUO received the B.Eng. degree in communication engineering from the Hebei University of Technology, Tianjin, China, in 2011. He is currently pursuing the Ph.D. degree with PLA Army Engineering University, China. His research interests include satellite communication and signal processing.

KAIJIE ZHOU received the B.Eng. degree in electrical engineering and automation from the Hefei University of Technology, Hefei, China, in 2007. He is currently pursuing the Ph.D. degree with PLA Army Engineering University, China. His research interests include satellite communication and signal processing.

HUALI WANG received the Ph.D. degree in electronic engineering from the Nanjing University of Science and Technology, China, in 1997. He is currently a Professor with the College of Communication Engineering, PLA Army Engineering University, China. His research interests include satellite communication and signal processing.

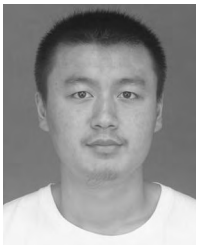

WANGHAN LV received the B.Eng. degree from the School of Electronic and Optical Engineering, Nanjing University of Science and Technology, China, in 2013, where he is currently pursuing the Ph.D. degree in electrical engineering. His research interests include sparse array signal processing and sparse sampling theory.